

# Stability of ZnO nanorods coated on the channel wall under continuous flow conditions

Berrin İkizler\*, Sümer Peker

Chemical Engineering Department, Ege University, 35100, Bornova, İzmir, Turkey

\*Corresponding author. Tel: (+90) 2323111495; Fax: (+90) 2323887776; E-mail: [berrin.ikizler@ege.edu.tr](mailto:berrin.ikizler@ege.edu.tr)

Received: 29 September 2013, Revised: 20 October 2013 and Accepted: 28 October 2013

## ABSTRACT

The damage given to the ZnO nanorod coating immobilized at the bottom of a rectangular channel by water flow is assessed in this work. The experiments were conducted in complete darkness to determine the inherent stability of the nanorod coating without the interfering effect of UV radiation. The quality and morphology of the nanorod arrays before and after use were determined by x-ray diffraction, scanning electron microscopy; rod breakage, by dynamic light scattering; and the extent of erosion, by concentration and weight measurements. The effect of pH of the flowing water in the range  $4 \leq \text{pH} \leq 10$ , and the effect of the volumetric flow rate in the range,  $3.3\text{--}33 \text{ cm}^3/\text{s}$  are investigated in this work as parameters. ZnO erosion reaches a low-level plateau in the pH range of  $6 \leq \text{pH} \leq 10$ . Within this range, water velocity and alignment of the nanorods control the extent of dissolution. Dissolution of ZnO nanorods essentially takes place on the polar (0001)-Zn plane of ZnO, resulting in the formation of serrated surfaces. Furthermore, inclined rods joining at the top surface is subjected to further dissolution through pit formation originating at the junction interface, and extending outwards. ZnO nanorod arrays could be used as a photocatalyst in the photocatalytic water treatment processes, where the dissolution from nanorods is in the range of 2.0–2.5 wt% after 24 h of operation under a flow rate of  $3.30 \text{ cm}^3/\text{s}$  ( $\approx 12 \text{ L/h}$ ), well under the requirements of World Health Organization. Copyright © 2014 VBRI press.

**Keywords:** ZnO nanorods; wurtzite; array characterization; coating stability; dissolution.



**Berrin İkizler** obtained her Ph. D. degree in 2012 from Ege University, İzmir, Turkey. She is currently working as a Research Assistant in the Department of Chemical Engineering in Ege University. Her research interests include synthesis of metal oxide nanoparticles, thin film deposition, growth of 1D nanorods, photocatalysts, photodegradation processes and fluid mechanics.



**Sümer Peker** has worked as a professor in the Chemical Engineering Department of Ege University. During her academic career, she has published three books, two of which are in the field of fluid mechanics; many articles on various aspects of interfacial phenomena, fluid mechanics and rheology. She has a patent on periodic controlled release from microcapsule/hydrogel composite systems.

## Introduction

ZnO is one of the promising semiconductor materials that are used in investigations of photocatalytic water treatment due to its wide and direct band gap of 3.37 eV and large excitonic binding energy of 60 meV. Band gap wavelength of ZnO includes a greater portion of the solar spectrum so its photocatalytic activity is sensitive to visible light [1-4]. In addition, it has higher activity in the degradation of certain dyes [2-4] and microorganisms [5]. Furthermore, its chemical stability and photocatalytic properties can be enhanced by doping with non-metals [6] or other semiconductors like  $\text{TiO}_2$  [7-9]. It is confirmed by various publications in the literature that, ZnO nanoparticles suspended in the pollutant medium shows a maximum photocatalytic activity (degradation efficiency greater than 95%) in the pH range of  $6 \leq \text{pH} \leq 11$  [1, 10-11]. However, the main drawback for widespread use of ZnO photocatalyst is its activity deterioration under strong acidic and alkaline environment due to dissolution, which limits the pH range in which it can be used [1, 10-13].

Although the influence of pH on the photocatalytic activity of ZnO catalyst was studied for various pollutants, rate of dissolution and the structural change of ZnO catalyst after the completion of photodegradation processes, have

not been investigated in detail. The stability of ZnO nanoparticles in terms of breakage and dissolution is crucial in water treatment applications. Separation and recovery of suspended catalyst particles broken from the nanoparticle array is an important process at the end of water treatment operation. If lost to the environment, ZnO nanoparticles are reported to be toxic to microorganisms in surface waters if their concentration exceeds a threshold value [14-17]. All the authors agree that the toxic effect of ZnO is due to solubilized  $\text{Zn}^{2+}$  ions. It is difficult to reach a general agreement on the threshold concentration, since zinc is an essential trace element beneficial to organisms up to a limiting concentration that varies with the type of the organism. A guideline by World Health Organization for allowable zinc concentration in drinking water from taps or in bottles is 3 mg/L [18-20]. This value, however, is not legally binding. United States Environmental Protection Agency National Primary Drinking Water Regulations assesses the zinc concentration as 5 mg/L [21].

Flow type photocatalytic reactors where the catalyst is immobilized on the walls of the reactor are recently developed technologies and ideally eliminate the separation and recovery of the catalyst nanoparticles at the end of the treatment process [9, 22-26]. In these types of reactors, water containing pollutants flow over the nanoparticles immobilized on reactor walls. The immobilization of the catalyst severely reduces the total available area of the nanoparticles, and brings the reaction under mass transfer control; that is, flow rate emerges as another parameter. The lifetime and the durability of the coating then become performance related issues that have to be resolved before the industrial use of these reactors [26-27]. Li et al. [27] evaluated critical research needs for photocatalytic water treatment to be performed in macro-scale equipment. One of these issues is the retention of nanomaterials to reduce operational costs related with nanoparticle loss and prevent humans and the environment from the risks associated with toxicity of these suspended particles or their solutions.

Although the assessment of stability of immobilized nanoparticles is a prerequisite for the determination of their viability for use in photocatalytic flow reactors, this subject is not investigated yet. The aim of this work is to investigate the chemical stability and durability of the ZnO nanorod coating on the channel walls under continuous flow conditions without the interfering effect of light and organic chemicals dissolved in water. The effect of pH and volumetric flow rate are studied as parameters to determine the dissolved amount from the ZnO nanorod coating and to assess the mechanism of nanorod erosion/dissolution.

## Experimental

### Materials

Zinc acetate dihydrate ( $\text{ZnAc}_2$ ), monoethanolamine (MEA), 2-methoxyethanol (2ME), zinc nitrate hexahydrate, ammonia ( $\text{NH}_3$ , 25 wt%), hydrochloric acid (HCl, 37 wt%) and sodium hydroxide (NaOH) were bought from Merck Company. All chemicals were of analytical grade and used without further purification. Distilled water, with a conductivity of 1.1  $\mu\text{S}/\text{cm}$  and pH value of 6.0, was used both in the preparation of solutions and in the stability experiments. Microscope glass slides with the dimensions

of  $26 \times 76 \times 1$  mm were bought from Marienfeld and used as substrates after cleaning ultrasonically in acetone, ethanol and distilled water each to remove surface impurities.

### Formation of ZnO seed layer on glass surfaces

ZnO nanorod arrays are formed on the glass substrates by a two-step process. At first, a thin ZnO seed layer is deposited on the glass plates using a sol-gel spin coating technique and then, ZnO nanorods are grown from this seed film by hydrothermal method.

The coating sol was prepared by mixing  $\text{ZnAc}_2$  in MEA and 2ME solution with a magnetic stirrer at  $60^\circ\text{C}$ , until a clear and homogeneous solution obtained. The molar ratio of  $\text{ZnAc}_2$  to MEA was kept at 1:1, with the concentration of  $\text{ZnAc}_2$  in the final solution as 0.5 mol/L. The coating sol was spin coated onto the clean substrate while rotating at 3000 rpm for 60 s and afterwards substrates was dried at  $150^\circ\text{C}$  for 30 min in an oven. The spin coating and drying procedure was repeated for five times to assure adequate coverage of the seeds on the substrate surface. After final annealing in air at  $450^\circ\text{C}$  for 1 h, the coated film was turned into ZnO seed film.

### Growth of ZnO nanorods

The substrates coated with the ZnO seed film were then immersed in an aqueous solution composed of 0.1 mol/L zinc nitrate and  $\text{NH}_3$  solution, at a molar ratio of  $\text{OH}^-/\text{Zn}^{2+}$ : 10/1. In a stainless steel autoclave, the growth temperature was kept constant at  $90^\circ\text{C}$  for growth duration of 1.5 h. The substrates coated with ZnO nanorods were thoroughly washed with distilled water and dried under ambient conditions. The dried substrates were weighed in order to calculate the net mass of the ZnO nanorod films.

### Characterization

The morphologies of the ZnO seed film and nanorod arrays were determined by Phillips XL-30S FEG field emission-scanning electron microscopy (SEM). The ZnO films coated on the plates are scanned at different points on the plate surface. Diameter, length and rod density distributions were measured from SEM images taken, using the Scandium (version 5.0) image analysis software. The crystalline structure of nanorods and seeds were determined using Phillips X'Pert Pro X-ray diffraction (XRD) with  $\text{CuK}\alpha$  radiation in a  $2\theta$  range from  $20^\circ$  to  $80^\circ$ .

### Stability of nanorods under flow conditions

A prototype continuous flow photocatalytic reactor in the shape of rectangular channel is designed by coating ZnO nanorod arrays on glass substrates forming part of the channel wall. The prototype flow reactor was constructed from Teflon material as a rectangular channel with the dimensions of width $\times$ length $\times$ height:  $2.6 \times 45 \times 0.2$  cm. ZnO nanorods grown on glass substrates served as a part of the bottom wall of the flow channel integrated in a continuous flow system. The chemical and mechanical stability of ZnO nanorods was studied as a function of flow rate and pH of flowing water. Flow set-up was covered to shield daylight and eliminate the effect of UV radiation. 1500 mL of distilled water was circulated by a peristaltic pump in the

flow system continuously for 24 hours at 25°C at the flow rates specified in **Table 1**. As the amount of ZnO removed from the substrates in one pass led to concentrations below the measurement range of the AAS, flowing water had to be recirculated over the coated substrates. pH of the water was adjusted by adding adequate amounts of 0.1 M HCl or 0.1 M NaOH solutions to a value in the range of 4–10 to investigate the pH effect. 5 mL samples were taken at certain time intervals and Zn<sup>2+</sup> ion concentration originating from the dissolution of ZnO nanorods were determined using VARIAN Spectra atomic absorption spectrophotometer (AAS). The assessment of ZnO nanorods broken from the array and suspended in water was done by dynamic light scattering (DLS, Malvern ZS) technique. On completion of the flow experiments, the total weight loss from the nanorod coating was also calculated from the difference in the weight of the dry plate before and after the flow experiment. The erosion of the nanorods was evaluated with SEM images.

**Table 1.** Volumetric flow rates and the corresponding velocities used in the flow system.

Q [cm <sup>3</sup> /s]	3.3	10	16	21	27	33
V [cm/s]	6.4	19	31	40	53	65

## Results and discussion

### Morphology of the seed layer and nanorods

Morphology of the seed films and nanorod arrays grown on these seeds are observed with SEM images shown in **Fig. 1**. The top view of the seeds developed after five layers of coating are given in **Fig. 1(a)**. The seeds have spherule shapes with locally jammed areas and an average diameter ( $D_{avg}$ ) of 31±9 nm. The thickness of the seed film is measured as 220 nm using the cross-sectional views of the SEM images (not shown here). The top and side views of the rods grown on the seed film are given in **Fig. 1(b)** and **(c)**, respectively. The rods are grown perpendicular to the plate surface with an average length of 4.18±0.17 μm. The appearance of perfect hexagons in the enlarged top view given in **Fig. 1(d)** indicates the one-dimensional hexagonal structure of the nanorods.

The statistical distribution of the diameters of the seeds and rods are obtained from the corresponding SEM images of **Fig. 1** and are given in **Fig. 2(a)** and **(b)**, respectively, in the form of histograms. There is a greater central tendency in the case of the seeds and except for the tailing toward the larger diameters that constitute a rather small fraction, the distribution is normally distributed around a mode value of 25–30 nm. Those apparently large diameter seeds may originate from the jamming together of small diameter seeds. The diameters of the rods are evidently much greater than that of the seeds, and are highly scattered with no central tendency. The average values obtained statistically from the SEM images are summarized in **Table 2**. The ratio of the number densities indicates that on the average, one rod grows over approximately 20 seeds. The implications and consequences of this ratio on the mechanism of dissolution will be delineated in the following sections of this paper. The length of the rods is uniform, the ratio of the

standard deviation of the length of the rods to the rod length (170/4180) being negligible with respect to that of the diameters (44/116). The outstanding feature of the nanorods is the large aspect ratio (L/D). The stability tests in the flow cell are done using plates whose coating characteristics are represented by the average values in **Table 2**.

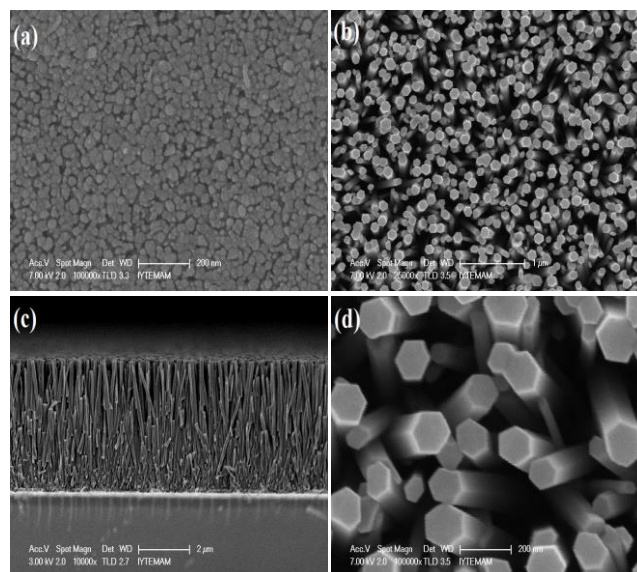


**Fig. 1.** The SEM images of the seeds and rods: (a) top view of seeds, (b) top view of the rods, (c) side view of the rods, and (d) the detail view of the rod surfaces.

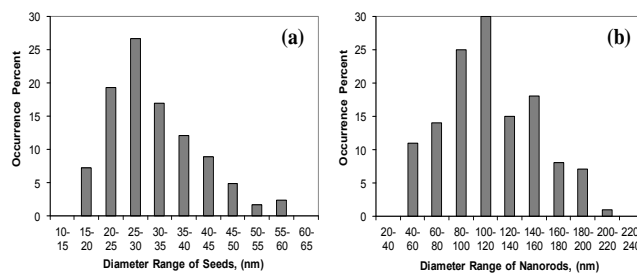


**Fig. 2.** The distribution of the diameters of the (a) seeds and (b) rods.

**Table 2.** The statistical values obtained from the SEM images.

	Number Density (#/cm <sup>2</sup> )	$D_{avg}$ (nm)	(L/D)	$D_{rod}/D_{seed}$	Seed Density/Rod Density (##)
<b>Seeds</b>	$9.59 \times 10^{10}$	31±9	-	3.7	19
<b>Rods</b>	$5.02 \times 10^9$	116±44	36		

### Crystal structure of the seed layer and nanorods

XRD pattern of the nanorods in comparison with that of the seeds are given in **Fig. 3**. Confirmation of the peaks with JPCDS No: 36-1451 standard shows that both the seeds and rods have exclusively wurtzite hexagonal crystalline structures. A single diffraction peak at  $2\theta = 34.42$  corresponding to (002) diffraction plane indicates highly

preferred orientation along c-axis, the growth direction normal to the plane surface. The intensity of the peak corresponding to nanorods issuing from the seed layer is more than hundredfold greater than that of the parent seeds indicating higher crystalline quality and unidirectional crystal growth of the nanorods in comparison with the seeds.

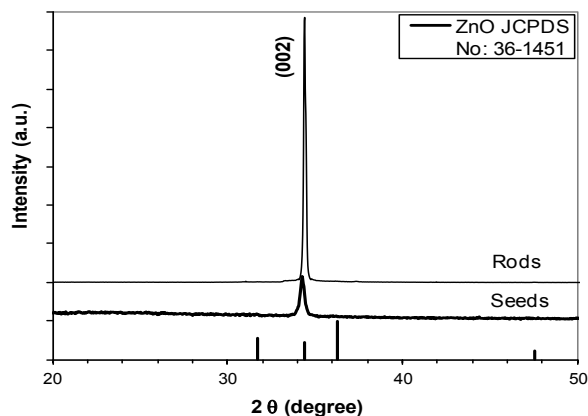
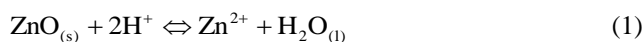


Fig. 3. XRD patterns of the rods and the seeds.

#### Effect of pH on the stability of the nanorods

The stability of nanorods is considered in terms of chemical and mechanical stability. Within the context of this work, *chemical stability* refers to the resistance against dissolution of ZnO nanorods coated at the bottom of the channel under continuous water flow with different pH. *Mechanical stability* is the resistance of nanorods against breakage and fracture under the shear stress exerted by the flowing water.

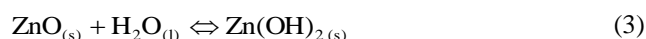
The factors affecting the stability of the nanorods were initially envisioned as the pH of the water flowing over the nanorod coating, and the water flow rate or velocity. The stability of ZnO nanorods is investigated in the pH range of 4 to 10, the range commonly encountered in surface waters, including the range  $6.5 < \text{pH} < 9.5$  for drinking water [28]. pH effect is examined at two different water flow rates ( $Q$ ), 10 and  $27 \text{ cm}^3/\text{s}$ . The former flow rate is well within the streamline flow range and the latter, near the upper limit before convective currents arise. The variation of zinc ion concentration in the flowing water as a function of time for a period of 24 hours is given in Fig. 4(a) and (b), for flow rates 10 and  $27 \text{ cm}^3/\text{s}$ . The pH of the water affects the adsorption of  $\text{H}^+$  or  $\text{OH}^-$  ions onto the surface of ZnO, which is followed by the dissolution of Zn from the surface of the nanorods by an ionic reaction [13]. It is generally agreed [13, 29-31] that the primary factor in the dissolution of ZnO is the  $\text{H}^+$  ion concentration of the flowing water according to equations (1) and (2).



It follows that the dissolution at  $\text{pH} = 4$  is increased regardless of the flow rates, though the dissolution is greater at higher flow rates. As the pH of the flowing water

increases,  $\text{H}^+$  ions become rare and the medium becomes electrostatically neutral, where the frequency of proton attacks is lowered. As the pH of the flowing water increases, both the total amount dissolved at the end of 24 hours and the rate of dissolution decreases, as given in Fig. 4. The concentration of the zinc ions in solution level off after approximately 8 hours, as neutral conditions are approached on depletion of the  $\text{H}^+$  and  $\text{OH}^-$  ions in water, measured with the pH meter.

Dissolution of ZnO could also take place in alkaline solutions by forming hydroxide complexes with  $\text{OH}^-$  [29-31]. However, as pH increases from 7.5 to 10, that is from neutral to weak alkaline solution, dissolution of nanorods continues to decrease and shows a minimum at  $\text{pH} = 10$ . Reichle et al. [31] has shown that at the isoelectric point of ZnO around  $\text{pH} = 10$ , the surface of the ZnO is electrically neutral and covered with  $\text{Zn}(\text{OH})_2$  through the reaction given by equation (3).



$\text{Zn}(\text{OH})_2$  has a very low solubility product of  $K_{\text{sp}} = 1.74 \times 10^{-17}$  at  $25^\circ\text{C}$ . Therefore,  $\text{Zn}(\text{OH})_2$  coverage of the ZnO surfaces could have prevented the ZnO nanorods from further dissolution by reaction with  $\text{OH}^-$  ions.

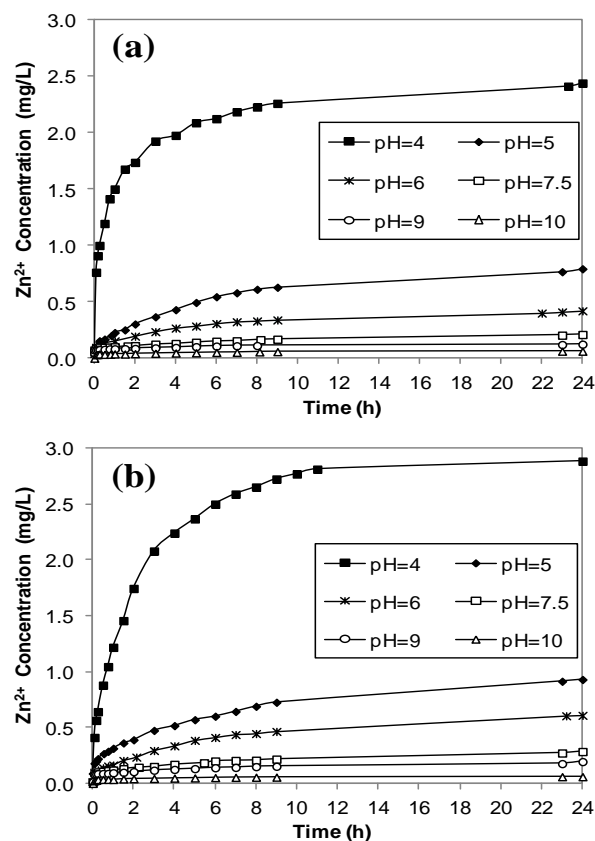


Fig. 4. The variation of the zinc ion concentration in the flowing water as a function of time over a period of 24 hours: (a)  $Q = 10 \text{ cm}^3/\text{s}$ , and (b)  $Q = 27 \text{ cm}^3/\text{s}$ .

The zinc ion concentrations reached at the end of 24 hours for each pH value in Fig. 4 is converted into the weight equivalent of ZnO and given in Fig. 5 in terms of

percent loss from the ZnO nanorod arrays for two different flow rates. The curves decrease sharply as the pH of the water increases from 4 to 5, and at a slower rate as the pH is increased further. Dissolution from ZnO does not increase significantly with an increase in the flow rate of water. The effect of water flow rate has a secondary importance when compared to pH of the medium, although, zinc ions could easily be removed from the surface of the rods as fast as they were formed.

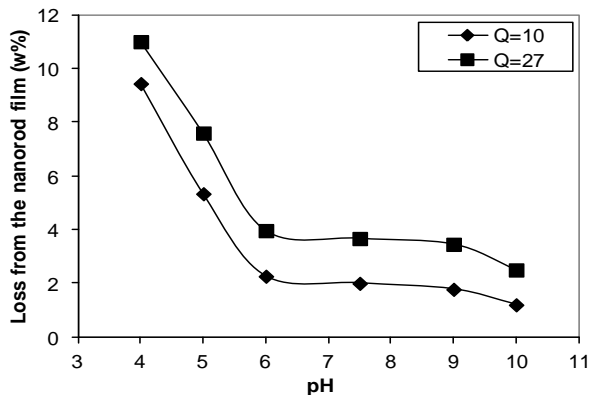


Fig. 5. Amount of ZnO removed at the end of 24 hours as a function of the pH of the circulating water.

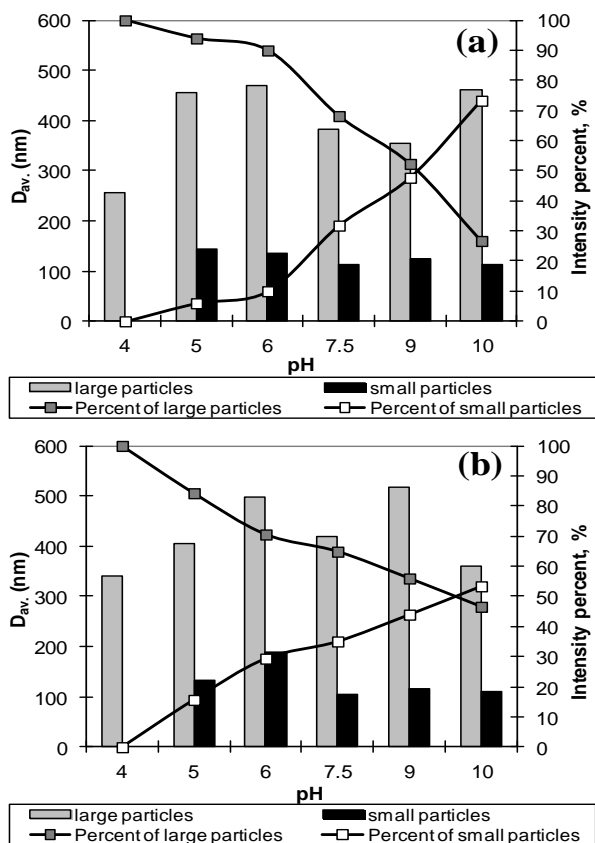


Fig. 6. DLS results showing the equivalent diameter of broken rods and percent distribution of these particles suspended in water: (a)  $Q=10 \text{ cm}^3/\text{s}$ , and (b)  $Q=27 \text{ cm}^3/\text{s}$ .

Information about the broken rods in suspension is obtained from DLS measurements. Bimodal distribution curves are obtained in these measurements, indicating the

existence of two size groups in the population of broken rods. The results are given in Fig. 6(a) and (b) for flow rates for 10 and  $27 \text{ cm}^3/\text{s}$ , where the values of the modes in DLS measurements are represented by gray and black bars for large and small diameter bars, respectively. The curves give the relative intensities for each distribution, indicating the percentages of the large and small particles in suspension. Since the DLS gives no information about the shape of suspended solids, but gives the equivalent diameter of a sphere ( $D_e$ ) calculated from the terminal velocity, no distinction can be made between rods broken at the seed/rod interface and agglomerated rod chips in suspension. From the average dimensions of the rods, the equivalent diameter of a typical rod could be calculated from  $(\pi D_e^3 / 6 = (4180 \text{ nm}) \times \pi (116 \text{ nm})^2 / 4)$  and equals to approximately 440 nm. The correspondence of the calculated and measured (gray bars) values implies that the rods in suspension were generally broken off at the seed/rod interface.

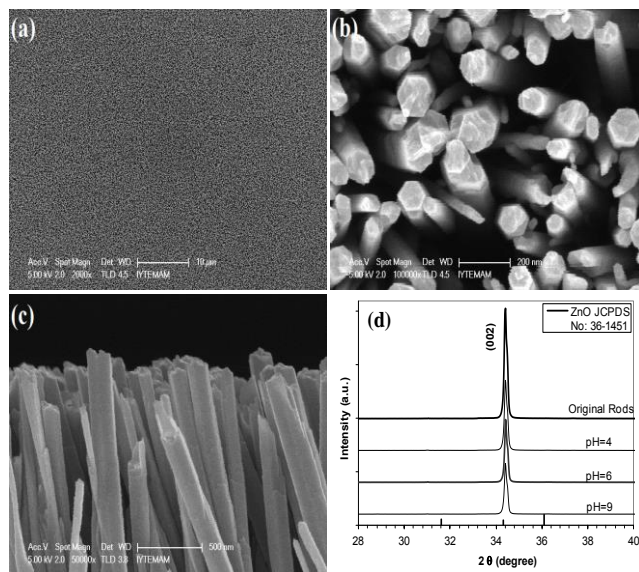
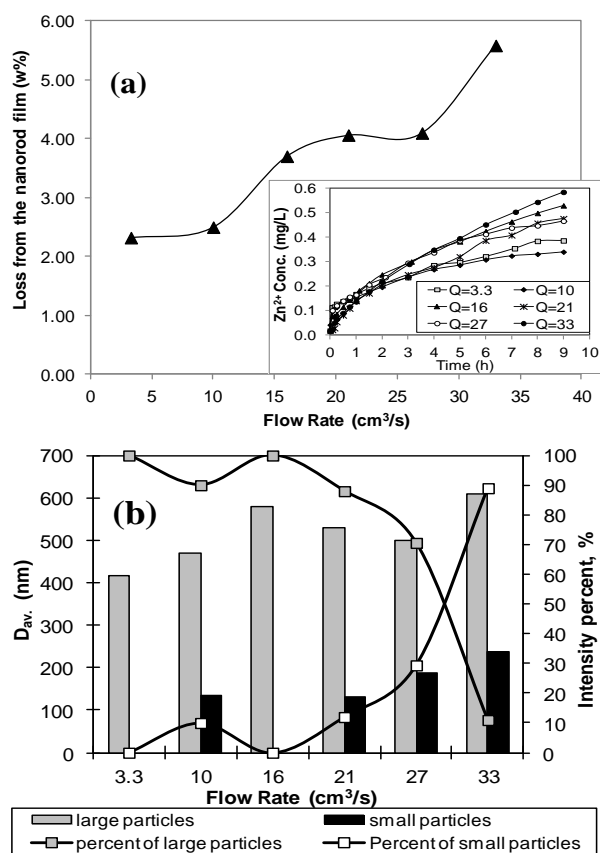


Fig. 7. The appearance of the ZnO nanorod arrays after 24 hours of water flow at pH=4 and  $Q=27 \text{ cm}^3/\text{s}$ : (a) general top view, (b) detail view of the rod surfaces, (c) side view, and (d) XRD pattern of the rods before and after flow experiment for different pH values at  $Q=27 \text{ cm}^3/\text{s}$ .

The diameter of the small particles remains approximately constant around 100–150 nm. These small particles could be small chipped-off rods or part of the rods broken along the fracture surfaces of rods. There are no small particles observed at pH=4 as indicated in Fig. 4. The broken rods in suspension probably dissolve during recirculation in the system as can be expected from the rapid dissolution rate at this pH. The percentage of the small particles increases as pH increases in Fig. 6, reflecting the decreased solubility of the suspended rods.

The SEM images given in Fig. 7 demonstrate the dissolution of ZnO and support the trends in Figs. 5 and 6. These images show the condition of the nanorod coating under the most severe conditions of pH=4 and high flow rates at  $Q=27 \text{ cm}^3/\text{s}$ . The overall view with a scale bar of 10  $\mu\text{m}$ , in Fig. 7(a), is representative of many images taken over the surface of the plate. The overall uniformity indicates that the adhesion of the rods to the surface of the

glass plate is quite strong and there is no patch wise removal in the macro scale. The top view of rods in **Fig. 7(b)** shows that most of the rods have eroded ends at their upper surface, the (0001)-Zn plane. The serrated end of the rods can be clearly observed in the side view images, shown in **Fig. 7(c)**. The existence of broken rods among the serrated rods at the back probably constitutes the small particles in suspension given in **Fig. 6**. The original XRD pattern of the rods together with the patterns of the rods damaged due to flow at different pH, given in **Fig. 7(d)**, differ in the intensity scale only, corroborating that the variations in the rods are due to erosion of the upper parts.



**Fig. 8.** The dissolution behavior of the nanorods in distilled water as a function of flow rate: (a) The amount removed at the end of 24 hours, inset: The variation of zinc ion concentration as a function of time, and (b) statistical distribution of the diameters of the suspended particles at the end of 24 hours.

#### Effect of water velocity

The effect of water velocity is investigated with distilled water at pH=6, without the addition of electrolytes for pH adjustment. The water flow rate is increased by an order of magnitude in this range, extending from completely streamline flow at  $Q=3.3 \text{ cm}^3/\text{s}$ , up to the limit of  $Q=33 \text{ cm}^3/\text{s}$  before convective currents arise, as given in **Table 1**. The dissolution of ZnO as a function of time is given in **Fig. 8(a)**, indicate a marked increase in the dissolution rate above  $Q > 10 \text{ cm}^3/\text{s}$ , pointing out the two mechanisms of dissolution. The variation of the total amount of ZnO removed at the end of 24 hours given in **Fig. 8(a)** implies interplay between the retention times of flowing water over the ZnO coated surface and hydrodynamic forces.

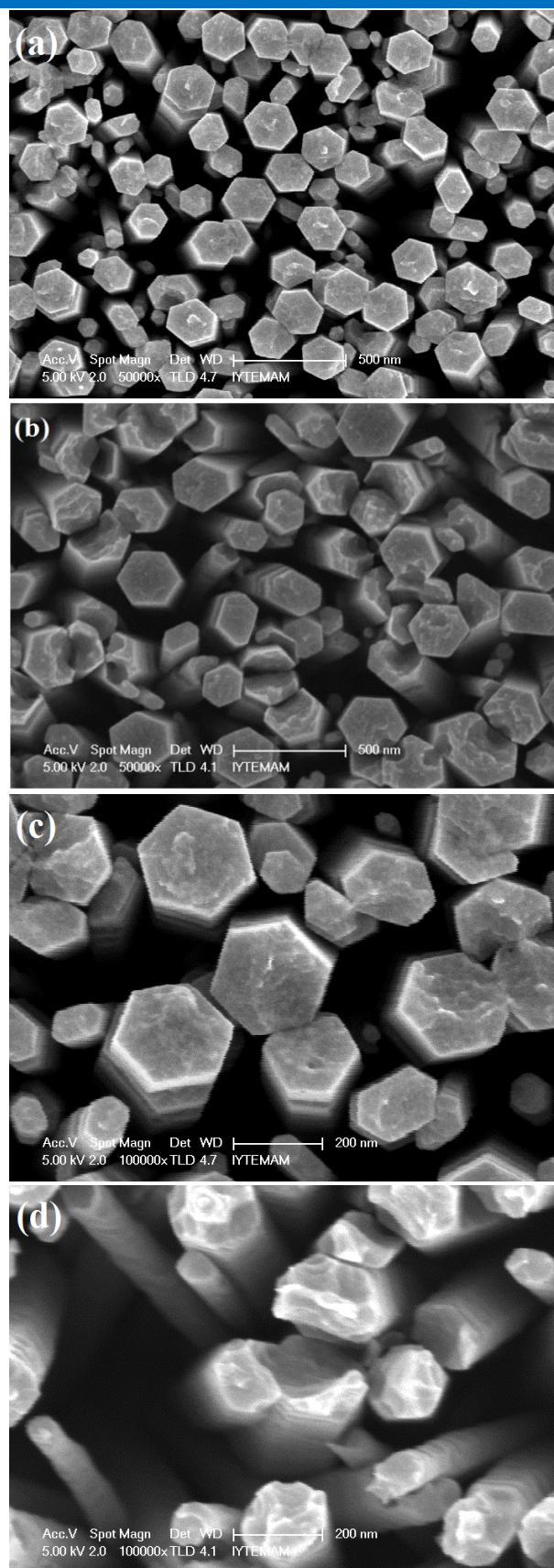


**Fig. 9.** SEM images of the nanorod coating after being subjected to water flow for 24 hours. (a) General view at  $Q=3.3 \text{ cm}^3/\text{s}$  and (b)  $Q=33 \text{ cm}^3/\text{s}$ ; close up view of the rods (c)  $Q=3.3 \text{ cm}^3/\text{s}$  and (d)  $Q=33 \text{ cm}^3/\text{s}$ .

At low flow rates, retention time of water over the coated surface is longer, leaving time for dissolution. On increasing the flow rate, retention time decreases, but the transfer rate of zinc ions from the ZnO surface to the bulk water increases, decreasing the mass transfer resistances to dissolution. Moreover, the shear stresses acting over the top surface of the nanorods facilitates the breakage of part of the rods along the fracture surfaces. The statistical distribution of the suspended rod particles measured with DLS is given in **Fig. 8(b)**. As the flow rate increases, the intensity of the large rods decreases and that of small chipped-off particles increases. The dissolution of the chipped-off rods also causes the irregularities in the curves of inset of **Fig. 8(a)**.

#### Mechanism of dissolution

Thermodynamically the most stable form of ZnO is wurtzite, with a hexagonal crystal structure. The top (0001) and bottom (000 $\bar{1}$ ) surfaces of the crystal are highly polar, whereas, the side surfaces are non-polar. The wettability of this polar surface brings about its preferential dissolution with respect to the other crystal surfaces [32]. The ZnO crystal is composed of Zn- and O- layers along the c- axis in the direction of which the growth rate is fastest. Dulub et al. [33-34] based on their observation with scanning tunneling microscopy, revealed that oxygen atoms along the edges of the (0001)-Zn surface could participate in acid/base reactions.

SEM images in **Fig. 9** indicate that a general dissolution of ZnO takes place at the reactive (0001)-Zn plane. The images were taken after the plate was subjected to flow with rates of 3.3 cm<sup>3</sup>/s and 33 cm<sup>3</sup>/s. Shear stresses acting on the rods are effective on the rate of ZnO dissolution. The greater the flow rate, the greater will be the velocity gradient and hence, the shear stresses that cause considerable erosion of the top surface at high flow rates as given in **Fig. 9(b)** and **(d)**.

Close-up views display that these apparently serrated surfaces form because of uneven erosion of exposed layers. In addition to general dissolution from the (0001)-Zn planes, effect of another mechanism is evident. The perfectly vertical rods that appear as hexagons in **Fig. 9(a)** and **(b)** are hardly affected by the water flow, whereas, the slanted rods that touch each other at the top surface of nanorod array are observed to be severely damaged by pit formation along the junction plane.

A possible mechanism for the development of tilted rods that initiates pit formation is the irregularities in the seed layer on which the rods grow. The statistical results given in **Table 2**, show that a hexagonal rod of average dimensions is anchored to approximately 20 seeds on which it grows. If the base seeds are homogeneous in terms of size and spatial distribution, then there is a high probability that the rods will be vertical. However, if some of the anchored seeds are longer than others, or if their spatial distribution is not uniform, then there is a high probability that the rods will grow in a slanted direction. When two slanting rods touch each other, the pattern of further crystallization will be highly perturbed, and the probability for the formation of dislocations will increase. These dislocations are favorable places for the attack of ions leading to dissolution

of ZnO. The abundance of these dislocations at the junction plane causes pit formation as disclosed in the detailed images in **Fig. 9(c)** and **(d)**.

#### Conclusion

Research on the stability of catalyst coating immobilized on channel walls is a prerequisite for the design and use of these reactors in water disinfection and decontamination, which this work addresses. Highly aligned ZnO nanorod arrays with large L/D ratios are tested for suitability as a coating in a prototype flow reactor. Erosion of the nanorod array is investigated as a function of the velocity and pH of flowing water. The damage given to the nanorod arrays showed that dissolution of ZnO nanorods essentially takes place on the polar (0001)-Zn plane of ZnO that is highly reactive, resulting in the formation of serrated surfaces. Furthermore, inclined rods joining at the top surface is subjected to further dissolution through pit formation starting from the junction interface. The dislocations and perturbations in the crystal lattice might be the cause for this carving-out effect. The results show that loss from immobilized ZnO nanorods could be reduced to acceptable levels in the pH range of 6-10 by improving the verticality of nanorods, and working at low flow rates (3-10 cm<sup>3</sup>/s) in the channel. Even in the extreme cases of pH=4 and at the start of convective current flow (33 cm<sup>3</sup>/s), dissolution of the ZnO nanorods after 24 hours as Zn<sup>2+</sup> is well below the allowable limits of 5 mg/L.

#### Acknowledgement

The authors gratefully acknowledge the financial support of the Scientific and Technological Research Council of Turkey extended through Grant 110M403.

#### Reference

- Pardeshi, S.K.; Patil, A.B. *J. Hazard. Mater.* **2009**, *163*, 403.  
DOI: [10.1016/j.jhazmat.2008.06.111](https://doi.org/10.1016/j.jhazmat.2008.06.111)
- Sakthivel, S.; Neppolian, B.; Shankar, M.V.; Arabindoo, B.; Palanichamy, M.; Murugesan, V. *Sol. Energy Mater. Sol. Cells* **2003**, *77*, 65.  
DOI: [10.1016/S0927-0248\(02\)00255-6](https://doi.org/10.1016/S0927-0248(02)00255-6)
- Kansal, S.K.; Singh, M.; Sud, D. *J. Hazard. Mater.* **2007**, *141*, 581.  
DOI: [10.1016/j.jhazmat.2006.07.035](https://doi.org/10.1016/j.jhazmat.2006.07.035)
- Dindar, B.; İçli, S. *J. Photochem. Photobiol., A* **2001**, *140*, 263.  
DOI: [10.1016/S1010-6030\(01\)00414-2](https://doi.org/10.1016/S1010-6030(01)00414-2)
- Aruoja, V.; Dubourguier H-C.; Kasemets, K.; Kahru, A. *Sci. Total Environ.* **2009**, *407*, 1461.  
DOI: [10.1016/j.scitotenv.2008.10.053](https://doi.org/10.1016/j.scitotenv.2008.10.053)
- Chen, L.C.; Tu, Y.J.; Wang, Y.S.; Kan, R.S.; Huang, C.M. *J. Photochem. Photobiol., A* **2008**, *199*, 170.  
DOI: [10.1016/j.jphotochem.2008.05.022](https://doi.org/10.1016/j.jphotochem.2008.05.022)
- Marci, G.; Augugliaro, V.; Lopez-Munoz, M.J.; Martin, C.; Palmisano, L.; Rives, V.; Schiavello, M.; Tilley, R.J.D.; Venezia, A.M. *J. Phys. Chem. B* **2001**, *105*, 1026.  
DOI: [10.1021/jp003172r](https://doi.org/10.1021/jp003172r)
- Marci, G.; Augugliaro, V.; Lopez-Munoz, M.J.; Martin, C.; Palmisano, L.; Rives, V.; Schiavello, M.; Tilley, R.J.D.; Venezia, A.M. *J. Phys. Chem. B* **2001**, *105*, 1033.  
DOI: [10.1021/jp003173j](https://doi.org/10.1021/jp003173j)
- He, Z.; Li, Y.; Zhang, Q.; Wang, H. *Appl. Catal. B* **2010**, *93*, 376.  
DOI: [10.1016/j.apcatb.2009.10.011](https://doi.org/10.1016/j.apcatb.2009.10.011)
- Daneshvar, N.; Rasoulifard, M.H.; Khataee, A.R.; Hosseinzadeh, F. *J. Hazard. Mater.* **2007**, *143*, 95.  
DOI: [10.1016/j.jhazmat.2006.08.072](https://doi.org/10.1016/j.jhazmat.2006.08.072)
- Nageswara Rao, A.; Sivasankar, B.; Sadasivam, V. *J. Mol. Catal. A: Chem.* **2009**, *306*, 77.

- DOI: [10.1016/j.molcata.2009.02.028](https://doi.org/10.1016/j.molcata.2009.02.028)
12. Yassitepe, E.; Yatmaz, H.C.; Öztürk, C.; Öztürk, K.; Duran, C. *J. Photochem. Photobiol., A* **2008**, *198*, 1.  
DOI: [10.1016/j.jphotochem.2008.02.007](https://doi.org/10.1016/j.jphotochem.2008.02.007)
  13. Han, J.; Qiu, W.; Gao, W. *J. Hazard. Mater.* **2010**, *178*, 115.  
DOI: [10.1016/j.jhazmat.2010.01.050](https://doi.org/10.1016/j.jhazmat.2010.01.050)
  14. Blinova, I.; Ivask, A.; Heinlaan, M.; Mortimer, M.; Kahru, A. *Environ. Pollut.* **2010**, *158*, 41.  
DOI: [10.1016/j.envpol.2009.08.017](https://doi.org/10.1016/j.envpol.2009.08.017)
  15. Franklin, N.M.; Rogers, N.J.; Apte, S.C.; Batley, G.E.; Gadd, G.E.; Casey, P.S. *Environ. Sci. Technol.* **2007**, *41*, 8484.  
DOI: [10.1021/es071445r](https://doi.org/10.1021/es071445r)
  16. Liu, G.; Wang, D.; Wang, J.; Mendoza, C. *Sci. Total Environ.* **2011**, *409*, 2852.  
DOI: [10.1016/j.scitotenv.2011.03.022](https://doi.org/10.1016/j.scitotenv.2011.03.022)
  17. Çeçen, F.; Semerci, N.; Geyik, A.G. *J. Chem. Technol. Biotechnol.* **2010**, *85*, 520.  
DOI: [10.1002/jctb.2321](https://doi.org/10.1002/jctb.2321)
  18. Birke, M.; Rauch, U.; Harazim, B.; Lorenz, H.; Glatte, W. *J. Geochem. Explor.* **2010**, *107*, 245.  
DOI: [10.1016/j.gexplo.2010.06.002](https://doi.org/10.1016/j.gexplo.2010.06.002)
  19. World Health Organization (WHO), Guidelines for Drinking-Water Quality-Health Criteria and other Supporting Information, 2<sup>nd</sup> ed., Geneva Switzerland, **1996**, Vol. 2, pp. 1-94.
  20. World Health Organization (WHO), Guidelines for Drinking-Water Quality-First Addendum to Third Edition, Recommendations. Geneva Switzerland, **2006**, Vol. 1, pp. 460.
  21. United States Environmental Protection Agency (US EPA) Office of Water, National Primary Drinking Water Standards, Washington D.C., **2003**, EPA 816-F-03-016. - Online: <http://www.epa.gov/safewater/consumer/pdf/mcl.pdf> (November 2006).
  22. Bahnemann, D. *Sol. Energy* **2004**, *77*, 445.  
DOI: [10.1016/j.solener.2004.03.031](https://doi.org/10.1016/j.solener.2004.03.031)
  23. Akyol, A.; Bayramoğlu, M. *J. Hazard. Mater.* **2010**, *180*, 466.  
DOI: [10.1016/j.jhazmat.2010.04.053](https://doi.org/10.1016/j.jhazmat.2010.04.053)
  24. Akyol, A.; Bayramoğlu, M. *J. Hazard. Mater.* **2010**, *175*, 484.  
DOI: [10.1016/j.jhazmat.2009.10.031](https://doi.org/10.1016/j.jhazmat.2009.10.031)
  25. Malato, S.; Fernández-Ibáñez, P.; Maldonado, M.I.; Blanco, J.; Gernjak, W. *Catal. Today* **2009**, *147*, 1.  
DOI: [10.1016/j.cattod.2009.06.018](https://doi.org/10.1016/j.cattod.2009.06.018)
  26. Chong, M.N.; Jin, B.; Chow, C.W.K.; Saint, C. *Water Res.* **2010**, *44*, 2997.  
DOI: [10.1016/j.watres.2010.02.039](https://doi.org/10.1016/j.watres.2010.02.039)
  27. Li, Q.; Mahendra, S.; Lyon, D.Y.; Brunet, L.; Liga, M.V.; Li, D.; Alvarez, P.J.J. *Water Res.* **2008**, *42*, 4591.  
DOI: [10.1016/j.watres.2008.08.015](https://doi.org/10.1016/j.watres.2008.08.015)
  28. EU Directive 1998/83/EC, Council Directive 98/83/EC of 3 November 1998 on the quality of water intended for human consumption. *Official Journal of the European Communities*, **1998**, L 330, 5.12.1998, 32.
  29. Fruhwirth, O.; Herzog, G.W.; Poullos, J. *Surf. Technol.* **1985**, *24*, 293.  
DOI: [10.1016/0376-4583\(85\)90079-2](https://doi.org/10.1016/0376-4583(85)90079-2)
  30. Degen, A.; Kosec, M. *J. Eur. Ceram. Soc.* **2000**, *20*, 667.  
DOI: [10.1016/S0955-2219\(99\)00203-4](https://doi.org/10.1016/S0955-2219(99)00203-4)
  31. Reichle, R.A.; McCurdy, K.G.; Hepler, L.G. *Can. J. Chem.* **1975**, *53*, 3841.  
DOI: [10.1139/v75-556](https://doi.org/10.1139/v75-556)
  32. Wöll, C. *Prog. Surf. Sci.* **2007**, *82*, 55.  
DOI: [10.1016/j.progsurf.2006.12.002](https://doi.org/10.1016/j.progsurf.2006.12.002)
  33. Dulub, O.; Boatner, L.A.; Diebold, U. *Surf. Sci.* **2002**, *519*, 201.  
DOI: [10.1016/S0039-6028\(02\)02211-2](https://doi.org/10.1016/S0039-6028(02)02211-2)
  34. Dulub, O.; Diebold, U.; Kresse, G. *Phys. Rev. Lett.* **2003**, *90*, 016102.  
DOI: [10.1103/PhysRevLett.90.016102](https://doi.org/10.1103/PhysRevLett.90.016102)

## Advanced Materials Letters

Publish your article in this journal

**ADVANCED MATERIALS Letters** is an international journal published quarterly. The journal is intended to provide top-quality peer-reviewed research papers in the fascinating field of materials science particularly in the area of structure, synthesis and processing, characterization, advanced-state properties, and applications of materials. All articles are indexed on various databases including [DOAJ](https://doi.org/10.1016/j.jphotochem.2008.02.007) and are available for download for free. The manuscript management system is completely electronic and has fast and fair peer-review process. The journal includes review articles, research articles, notes, letter to editor and short communications.

JOURNAL  
**VBRI Press**  
a rapid publication platform

